1-1-2012

Globular reduced graphene oxide-metal oxide structures for energy storage applications

Alfred Chidembo
University of Wollongong, atc987@uowmail.edu.au

Seyed Hamed Aboutalebi
University of Wollongong, sha942@uowmail.edu.au

Konstantin Konstantinov
University of Wollongong, konstan@uow.edu.au

Maryam Salari
University of Wollongong, msalari@uow.edu.au

Brad R. Winton
University of Wollongong, bwinton@uow.edu.au

See next page for additional authors

Journal Name

Dynamic Article Links ►

Cite this: DOI: 10.1039/c0xx00000x

www.rsc.org/xxxxxx

ARTICLE TYPE

Globular Graphene Oxide-Metal Oxide Structures for Energy Storage Applications

Alfred Chidembo,[a] Seyed Hamed Aboutalebi,[a] Konstantin Konstantinov,*[a] Maryam Salari,[a] Brad Winton,[a] Ivan Nevirtcovets [a] and Hua Kun Liu[a,b]

Received (in XXX, XXX) Xth XXXXXXXXX 20XX, Accepted Xth XXXXXXXXX 20XX
DOI: 10.1039/b000000x

In this work, we employed an in-situ spray pyrolysis approach to fabricate metal oxide-graphene composites with highly porous morphologies. The materials exhibited unique globular lettuce-like structures comprising metal oxide nanoparticles embedded between graphene sheets with high capacitance.

Supercapacitors along with Li-ion battery research have experienced a massive growth over the past few years due to the emergent demand for cleaner energy storage devices. The main focus has been directed towards portable energy devices and hybrid vehicles. Despite the massive attention, the challenge for these devices has been the development of functional materials that enhance the overall performance of the electrodes. Although a large variety of energy storage materials used in Li-ion batteries and supercapacitors have been reported, these still have their limitations.

Supercapacitors operate on almost the same principle as batteries. However, the charge storage mechanisms of the two devices differ. While supercapacitors store energy by charge separation, batteries rely on chemical energy stored in the bulk of the electrode material which is a limiting factor for long cycle life and fast charging [1]. Supercapacitors have much longer cycle life, fast charge and higher power density than batteries, although their energy density is still very low making them heavy and bulky.

To overcome this problem, today's research focuses on two main fronts. The first one is the combination of pseudocapacitor (metal oxides) and EDL (carbonaceous materials) materials while the second focuses on the engineering of new structures and morphologies. Both approaches allow us to maximise the materials performance almost reaching their theoretical capacitances.

Since the discovery of graphene, a new generation of nano materials and composites based on metal oxides (MO), graphene [2],graphene oxide (GO) [3] and reduced graphene oxide (rGO) [4] have being intensively studied. These materials, apart from being less bulky, offer an enhanced surface area and good cycling stability for both supercapacitors and batteries [5]. Many authors have reported methods for engineering of GO/MO nanocomposites [3, 6], such as co-precipitation and template methods [7] or hydrothermal based technology [8], where the obtained materials generally consist of randomly mixed structures. To address this problem, some groups have recently investigated surfactant directed self-assembly [9], layer-by-layer deposition [10] and other techniques such as liquid crystalline route [11] to prepare layered materials but these methods are either time-consuming and/or difficult for bulk-materials synthesis. Moreover, there are still obstacles involved in the large-scale fabrication of these composites which render them impractical for real applications. Therefore, the engineering and development of ordered particles on a large-scale is still an unstudied field.

In the present paper we report the large scale engineering of globularly shaped rGO-MO nanocomposites (MO = Co_3O_4 or NiO) using an efficient and versatile in-situ spray pyrolysis approach. These structures demonstrate superior energy storage performance and good structural stability after cycling. We show that this approach can be applied to a range of metal oxide materials and demonstrate that the electrochemical properties can be much improved. Previously, we [12] demonstrated the advantages of the spray pyrolysis engineering to obtain other type of Si/Carbon composites with superior performance as anode material in Li-ion batteries.

Graphene oxide for the composites in this work was prepared in the same way as earlier reported in our work [11a]. To obtain the composites, cobalt hydroxide ($Co(OH)_2$, 95%, Aldrich) powder was dissolved in 1 M nitric acid solution. The solution was then added into a diluted GO dispersion in water and stirred for 30 minutes using a magnetic stirrer. The hybrid materials were then obtained in situ by spraypyrolyzing the suspension into a vertical type spray pyrolysis reactor to obtain 20% rGO-Co_3O_4 composite. The same procedure was performed for the preparation of the rGO-NiO composite. Details of all experimental procedures, electrode preparation and characterization methods are outlined in the supporting information.

The structure of the obtained hybrid composite was evaluated employing X-ray diffraction and Scanning electron microscopy techniques. All the diffraction peaks of both rGO–Co_3O_4 and rGO-NiO were perfectly indexed to cubic Co_3O_4 and NiO structures (see Figure S1 in supporting information). Additionally, no peak of graphene was detected thus suggesting that graphene sheets were homogeneously dispersed in the composite [13]. This was also supported by the EDS mapping for the rGO-Co_3O_4 composite (See Figure S2 in supporting information).

Being amphiphilic in nature [11a, 11b], the hydrophilic parts of GO

sheets can quite easily interact with hydrophilic metal nitrates resulting in strong bonding between GO sheets and the starting precursor.

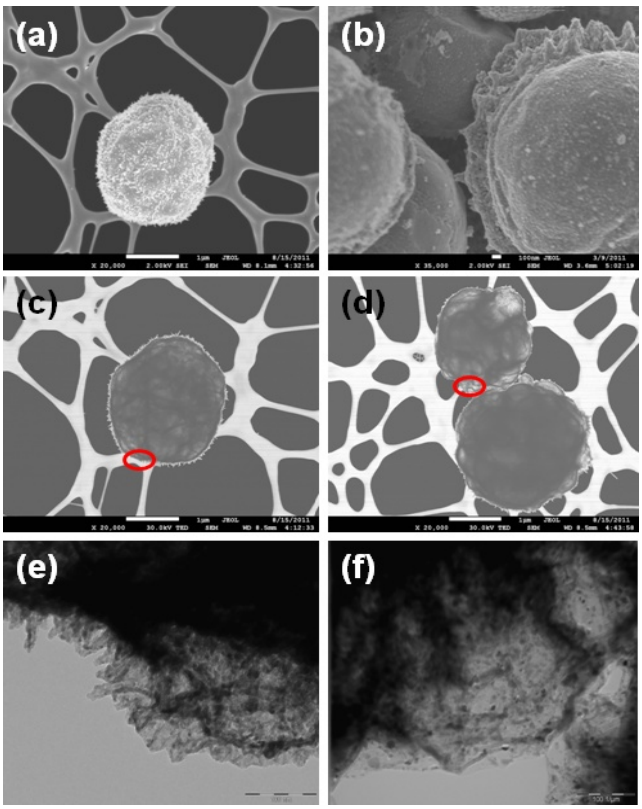

Fig.1 SEM images of (a) Co_3O_4 and (b) NiO after spraying. TEM images of rGO-Co_3O_4 and rGO-NiO composites with highlighted areas expanded in figures (e) and (f).

Therefore, the nucleation and growth of MO nanocrystals during the spray pyrolysis take place predominantly on the surface of GO sheets. The solid matrix of graphene then prevents these particles from excessive coagulation and coalescence into larger aggregates. Furthermore, the reduction of GO to rGO occurs during the process and this is confirmed by XPS spectra (see Figure S3 in supporting information).

The introduction of large GO sheets which are typically in the size of 30 µm [11b], resulted in the formation of composite globules. (Figure 1a, b). HRSEM was used to investigate the morphology of the composites. In figure 1 a and b, the rough globular surface due to the presence of nanoparticles and porous nature of the MO contribute significantly to the overall electrochemical performance of the materials. This structure allows the penetration by the electrolyte and consequently facilitating Faradaic reactions. The incorporation of larger rGO sheets (Figure 1a) in the composite structure which are observed to form a lettuce-like structure is also advantageous in terms of enhanced electrical conductivity. Additionally, their presence leads to an increase in both double layer capacitance and electrochemical stability of the composites.

The typical TEM images, shown in Figures 1c and d reveal the globular lettuce-like structure of the composite particles. The images in low magnification (Figures 1c and d) elucidate the envelopment of MO particles within bended rGO sheets resulting in the formation of an interconnected three dimensional network structure. This interconnected structure offers the unique advantages of both introducing conductive pathways through the whole structure and simultaneously improving the mechanical strength of the final composite. It can also be observed from the highlighted areas in Figures 1c and 1d in high magnification (Figures 1e and f) that metal oxide nanoparticles grown on rGO sheets are quite homogeneously and densely distributed.

The graphene encapsulated spheres showed crinkled and rough textures that were associated with the presence of flexible and ultrathin graphene sheets. Although, it is almost impossible to rule out the possibility of some degree of restacking of reduced graphene oxide sheets into graphene stacks during the spray pyrolysis process, TEM observation of the edge of one individual globular structure demonstrated the monolayer nature of rGO obtained by this method. Nevertheless, an ordered, layered nanostructure with metal oxide and the graphene materials is formed.

This particular arrangement is responsible for the high capacitive behaviour as the contribution of pseudocapacitance of the MO and double layer contribution of the carbonaceous material is exploited. Furthermore, rGO provides good conductivity which is supported by the small charge transfer resistance shown in the Nyquist plots.

Cyclic voltammetry was used as the first diagnostic test to study the electrochemical properties of the composites. Figure 2 shows CV results with figure 2(a) and (b) showing the individual CV curves for the two rGO-MO nanocomposites.

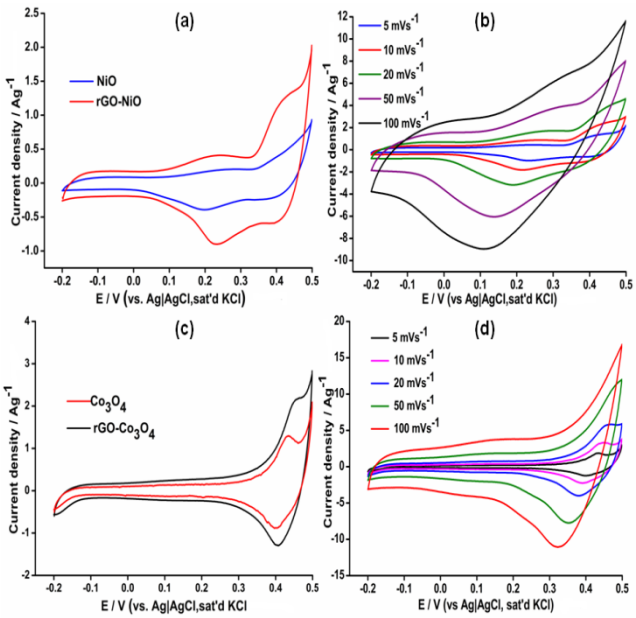

Fig.2 Comparative CVs at 5mVs^{-1} (a) and (c). Variation of specific capacitance with scan rate (b) and (d) for the rGO-MO composites.

From figure 2(a) the cyclic voltammograms for both NiO and rGO-NiO nanocomposite show redox peaks at 0.45 V and 0.22 V due to the $Ni(OH)_2$/NiOOH redox reaction[14] [15]. These peaks are accompanied by a broad shoulder peak between 0.1 and 0.35 V probably due to oxygenated groups on the rGO. In Figure 2(b),

redox peaks observed for rGO-Co_3O_4 are believed to be from reactions reported earlier [6b]. The effect of the rGO is clearly visible from the increase in background current in the CVs.

Both the rGO-MO CVs deviate from the rectangular shape expected for typical EDLCs. This is due to the pseudocapacitance contribution from the metal oxides as reduced graphene oxide has a capacity of about 205 Fg^{-1} [16]. The large current separation therefore indicates increased capacitive behaviour which was calculated by integrating the area covered by the CV [11a]. A total capacitance of 687 Fg^{-1} was obtained for the rGO-Co_3O_4 composite while that of rGO-NiO was 656 Fg^{-1} composite at 5 mVs^{-1} which is much higher compared to other graphene based supercapacitors reported in literature (Table 1).

Table 1. Graphene based composites used for supercapacitors.

Composite	Electrolyte	Method of preparation	Specific capacitance (Fg^{-1})	Ref.
rGO-Co_3O_4	1 M KOH	Spray Pyrolysis	687	Current study
rGO-Co_3O_4	6 M KOH	Surfactant and post annealing	163.8	[4]
GNS-Co_3O_4	6 M KOH	Microwave assisted method	243.2	[17]
Graphene – Co_3O_4	2 M KOH	In-situ solution based method	478	[18]
Graphene-MnO_2	1 M Na_2SO_4	Microwave Irradiation	310	[6a]
rGO- NiO	1 M KOH	Spray Pyrolysis	656	Current study
GO-NiO	1 M KOH	Electrophoretic deposition and chemical-bath deposition	400	[19]
Graphene Sheet-RuO_2	1 M H_2SO_4	Sol-gel + low temperature annealing	570	[6c]
GO-SnO_2	1 M KCl	ultrasonic spray pyrolysis	42.7	[20]
GO-ZnO	1 M KCl	ultrasonic spray pyrolysis	61.7	[20]

The charge storage mechanism of the two metal oxides has been described in previous reports as being analogous [21]. The spray pyrolysis route enables excellent encapsulation of metal-oxide particles within graphene sheets thus leading to remarkable performance and cyclability. Graphene clearly enhances the electrochemical properties of the nanocomposites by first acting as a conductive support ideal for electron and ion transportation. Secondly, the graphene capsule stabilizes the electrode structure with a good electric contact between the metal oxide particles and conductive graphene during the charge−discharge process.

Additional tests showed a reduction in capacitance with increase in scan rate being more pronounced for the NiO composite while the rGO-Co_3O_4 shows better capacitance retention (see Figure S4 a and b in supporting information). A specific capacitance of 580 Fg^{-1} for rGO-Co_3O_4 at 100 mVs^{-1} reflects good rate capacity and power density. We therefore concluded that the three-dimensional conducting network formed by the interaction between Co_3O_4 particles and graphene oxide, coupled with the high porosity of the composite facilitated OH^- soaking into the bulk material. This resulted in a decrease in the ionic and electronic transportation distances thus improving the electrode kinetics consequently enhancing the rate capability [22].

rGO-NiO electrodes showed poor rate capability due to the insertion of OH^- ions being limited to the electrode surface. The inner active sites within the electrode therefore do not get accessed at high scan rates by the electrolyte and cannot precede the redox transitions completely. Both electrodes however, show ideal capacitive behaviour as shown in the plots for current density vs. scan rate (see Figure S4c and d) in supporting information).

Electrochemical impedance spectroscopy tests were performed for both rGO-MO electrodes to understand the capacitive behaviour and resistance associated with the electrodes. Supercapacitors generally behave as pure resistors at high frequencies and typical capacitors at low frequencies.

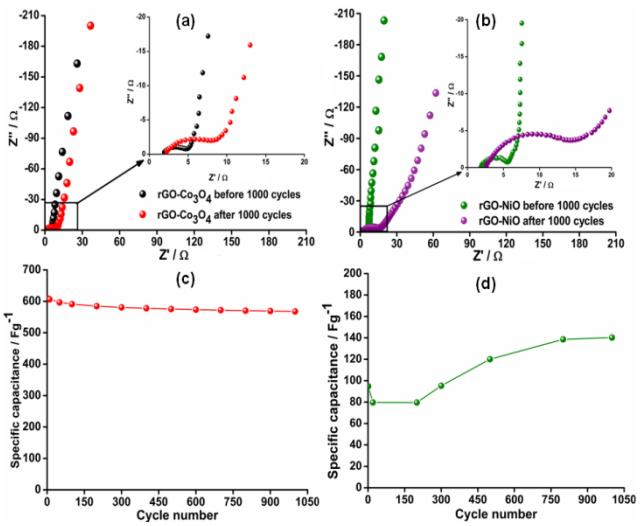

Fig.3 (a) Nyquist plots for GO-Co_3O_4 composite before and after 1000 cycles. (b) Nyquist plots for GO-NiO composite before and after 1000 cycles. (Inset: expanded high frequency region). Variation of specific capacitance with cycle number for GO-Co_3O_4 (c) and GO-NiO (d) obtained at 50 mVs^{-1}.

In the high frequency region, a semicircle due to charge transfer resistance on the electrode/electrolyte interface is observed. The region between the high frequency and low frequency regions is called the Warburg region and this is a combination of both resistive and capacitive behaviour characterized by diffusive resistance. The low frequency region is mainly characterized by purely capacitive behaviour. The Nyquist plots generated from the impedance data for the composites are shown in Figure 3. Both impedance spectra are similar, exhibiting the characteristic high frequency region semicircle and low frequency vertical line. The insets show the expanded high frequency region where in both figures, an increase in the semicircle radius implying an increase in the R_{ct} with increase in scan number is highlighted.

At low frequencies, the Nyquist plots become more vertical, implying purely capacitive behaviour. However, after 1000 cycles the slopes decrease towards an angle of 45° implying a decrease in the phase angle and a deviation from ideal capacitive behaviour and a domination of Warburg diffusion.

Cyclic voltammetry was employed to determine the stability of

the rGO-MO composites at 50 mVs^{-1}. As shown in figure 3 b the specific capacitance for the rGO-Co_3O_4 electrode decreased by 6.9 % demonstrating ideal stability for supercapacitors. Interestingly, the specific capacitance of the rGO-NiO electrode increased gradually by 48% of the initial value during the first 600 cycles. This is a due to the activation of the rGO-NiO active material. This phenomenon has also been observed by Yuan et al. [14]. The stability profiles of the two electrode materials entail the suitability of the materials for practical supercapacitor electrodes.

Conclusions

In conclusion, we have synthesized globularly shaped rGO-MO composites with high performance for supercapacitor electrodes using spray pyrolysis method. Additionally, the spray pyrolysis method proved to be an efficient method to effectively encapsulate MO particles with rGO simultaneously. The resulting composites exploit the benefits of pseudocapacitive nature of the metal oxide and conductive EDLC nature of the rGO. The technique also presents an opportunity to produce industry scalable ordered rGO-MO composites using a variety of metal oxides for both batteries and supercapacitors.

Acknowledgements

The authors thank the Australian Research Council for the financial support provided through DP (1093952). The authors thank Dr. Sima Aminorroaya-Yamini for assistance with SEM.

Notes and references

[a] *Institute for Superconducting & Electronic Materials (ISEM), Innovation Campus, University of Wollongong, Wollongong, NSW 2519, Australia, Fax: 0061242215731; Tel: 0061242215730; E-mail: konstan@uow.edu.au*

[b] *ARC Centre of Excellence in Electromaterials Sciences, Institute for Superconducting & Electronic Materials (ISEM), Innovation Campus, University of Wollongong, Wollongong, NSW 2519, Australia, Fax: 0061242215731; Tel: 0061242215730; E-mail: hua@uow.edu.au*

† Electronic Supplementary Information (ESI) available: [details of any supplementary information available should be included here]. See DOI: 10.1039/b000000x/

‡ Footnotes should appear here. These might include comments relevant to but not central to the matter under discussion, limited experimental and spectral data, and crystallographic data.

[1] M. Winter, R. J. Brodd, *Chemical Reviews* **2004**, *104*, 4245.

[2] H. M. Jeong, J. W. Lee, W. H. Shin, Y. J. Choi, H. J. Shin, J. K. Kang, J. W. Choi, *Nano Letters* **2011**, *11*, 2472.

[3] S. Chen, J. Zhu, X. Wu, Q. Han, X. Wang, *ACS Nano* **2010**, *4*, 2822.

[4] W. Zhou, J. Liu, T. Chen, K. S. Tan, X. Jia, Z. Luo, C. Cong, H. Yang, C. M. Li, T. Yu, *Physical Chemistry Chemical Physics* **2011**, *13*, 14462.

[5] E. Yoo, J. Kim, E. Hosono, H.-s. Zhou, T. Kudo, I. Honma, *Nano Letters* **2008**, *8*, 2277.

[6] a)J. Yan, Z. Fan, T. Wei, W. Qian, M. Zhang, F. Wei, *Carbon* **2010**, *48*, 3825; b)X.-h. Xia, J.-p. Tu, Y.-j. Mai, X.-l. Wang, C.-d. Gu, X.-b. Zhao, *Journal of Materials Chemistry* **2011**, *21*, 9319; c)Z.-S. Wu, D.-W. Wang, W. Ren, J. Zhao, G. Zhou, F. Li, H.-M. Cheng, *Advanced Functional Materials* **2010**, *20*, 3595.

[7] H.-W. Wang, Z.-A. Hu, Y.-Q. Chang, Y.-L. Chen, H.-Y. Wu, Z.-Y. Zhang, Y.-Y. Yang, *Journal of Materials Chemistry* **2011**, *21*, 10504.

[8] X. Yang, C. Lu, J. Qin, R. Zhang, H. Tang, H. Song, *Materials Letters* **2011**, *65*, 2341.

[9] D. Wang, R. Kou, D. Choi, Z. Yang, Z. Nie, J. Li, L. V. Saraf, D. Hu, J. Zhang, G. L. Graff, J. Liu, M. A. Pope, I. A. Aksay, *ACS Nano* **2010**, *4*, 1587.

[10] X. Li, G. Zhang, X. Bai, X. Sun, X. Wang, E. Wang, H. Dai, *Nat Nano* **2008**, *3*, 538.

[11] a)S. H. Aboutalebi, A. T. Chidembo, M. Salari, K. Konstantinov, D. Wexler, H. K. Liu, S. X. Dou, *Energy & Environmental Science* **2011**, *4*, 1855; b)S. H. Aboutalebi, M. M. Gudarzi, Q. B. Zheng, J.-K. Kim, *Advanced Functional Materials* **2011**, *21*, 2978; c)J. E. Kim, T. H. Han, S. H. Lee, J. Y. Kim, C. W. Ahn, J. M. Yun, S. O. Kim, *Angewandte Chemie International Edition* **2011**, *50*, 3043.

[12] S.-H. Ng, J. Wang, D. Wexler, K. Konstantinov, Z.-P. Guo, H.-K. Liu, *Angewandte Chemie International Edition* **2006**, *45*, 6896.

[13] S. Yang, X. Feng, S. Ivanovici, K. Müllen, *Angewandte Chemie International Edition* **2010**, *49*, 8408.

[14] C. Yuan, X. Zhang, L. Su, B. Gao, L. Shen, *Journal of Materials Chemistry* **2009**, *19*, 5772.

[15] M.-S. Wu, Y.-A. Huang, C.-H. Yang, J.-J. Jow, *International Journal of Hydrogen Energy* **2007**, *32*, 4153.

[16] Y. Wang, Z. Shi, Y. Huang, Y. Ma, C. Wang, M. Chen, Y. Chen, *The Journal of Physical Chemistry C* **2009**, *113*, 13103.

[17] J. Yan, T. Wei, W. Qiao, B. Shao, Q. Zhao, L. Zhang, Z. Fan, *Electrochimica Acta* **2010**, *55*, 6973.

[18] B. Wang, Y. Wang, J. Park, H. Ahn, G. Wang, *Journal of Alloys and Compounds* **2011**, *509*, 7778.

[19] X. Xia, J. Tu, Y. Mai, R. Chen, X. Wang, C. Gu, X. Zhao, *Chemistry – A European Journal* **2011**, *17*, 10898.

[20] T. Lu, Y. Zhang, H. Li, L. Pan, Y. Li, Z. Sun, *Electrochimica Acta*, **2010**, *55*, 4170.

[21] V. Srinivasan, J. W. Weidner, *Journal of Power Sources* **2002**, *108*, 15.

[22] J. Lang, X. Yan, Q. Xue, *Journal of Power Sources* **2011**, *196*, 7841.

